Available online at www.CivileJournal.org

Civil Engineering Journal

(E-ISSN: 2476-3055; ISSN: 2676-6957)

Vol. 11, No. 02, February, 2025

Sedimentation Characteristics and Sediment Transport in the Palu River Estuary

Adi Sucipto [1*], M. Arsyad Thaha [1], M. Putra Hatta [1], Faisal Mahmuddin [2]

[1] *Department of Civil Engineering, Hasanuddin University, South Sulawesi 91711, Indonesia.*

[2] *Department of Marine Engineering, Hasanuddin University, South Sulawesi 91711, Indonesia.*

Received 21 October 2024; Revised 07 December 2024; Accepted 19 December 2024; Published 01 February 2025

Abstract

Sedimentation is the process through which materials transported by water flow settle within that water. Changes in current patterns, driven by tides and variations in current velocity, can influence sediment transport. This study aimed to identify sediment transport patterns and analyze the characteristics of suspended sediment and bed load in the Palu River estuary. We employed field investigations, two-dimensional (2D) numerical modeling, and data analysis to process the findings. The results indicated that the sediment characteristics in the Palu River estuary varied, with a predominance of sand and gravelly sand. Additionally, sediment transportation patterns were found to be primarily influenced by river flow discharge rather than tidal effects. The research findings are presented in a correlation equation that illustrates the relationship between dimensionless parameters: $C = \rho_s.(a.\psi)^b$ with coefficient values of a = 412.71 and b = (-0.545). The results of this correlation equation indicate that as the energy from water movement increases, sediment becomes more dispersed, leading to changes in the concentration of sediment particles. It can be concluded that various variables affect sediment transport due to hydrodynamic conditions.

Keywords: Sedimentation; Sediment Transport; Palu River.

1. Introduction

Palu Bay is located on the north coast of Sulawesi, extending from the south between 0°53'9.32" S and 0°38'41.21' E, with the eastern and western boundaries at 119°52'58.27' E and 119°44'19.50" E, respectively. Meanwhile, the capital of Central Sulawesi Province, Palu City, is geographically located at the southern end of the bay [1]. The coastal waters near the Palu River estuary hold potential for the social and economic development of local communities [2]. The Palu River is experiencing a significant problem with sedimentation. This issue is primarily caused by erosion linked to changes in land cover in the river's upstream areas. These changes lead to increased fluctuations in river discharge, which subsequently result in sediment accumulating in the river channel and estuary. The impact occurs when the river's profile cannot handle a sufficiently large flow discharge, leading to significant sediment being carried by the water. This sedimentation results in obstacles forming within the river channel, which can potentially cause flooding in the downstream areas.

Sediment is crucial in every aquatic ecosystem [3]. Sediment transport material originates from eroded regions in the watershed and enters the water through hydrodynamic processes [4]. Sediments in estuarine and coastal waters can distribute and pollute marine environments. The dispersion of sediments in the water column occurs due to the influence of waves and currents, which can increase turbidity and accelerate sediment deposition [5]. The concentration of

* Corresponding author: adisucipto.dk6@gmail.com

http://dx.doi.org/10.28991/CEJ-2025-011-02-03

sediment entering the water can impact sedimentation, leading to changes in the morphology of the riverbed. This happens when the flow rate is slower than the velocity at which sediments move [6]. Thus, the flow velocity plays a significant role in the movement of sediment within the water [7]. Changes in the natural shape of riverbeds can have a significant impact on the river environment and its structure [8].

Sediment transport analysis requires flow data; thus, analyzing the flow and the influence of tides on flow velocity at the river's mouth is necessary [9]. Tidal processes and river discharge in estuaries can transport sediment loads and create variations in the density of sea water and river water. These differences can lead to siltation caused by sedimentation flowing downstream. Factors such as particle size, specific gravity, fall velocity, and the volume of water flowing through the river can all influence sedimentation rates. Sediment transport happens through two main processes: bedload and suspended load [10]. Sediment drift originates from sediment loads transported by rivers to estuaries and beaches, significantly affecting the decline in water quality physically, chemically, and biologically [11, 12]. High sediment transport will occur in the meeting area between the river and the sea due to low flow velocity, leading to sedimentation of the transported material. Research by Herman et al. [13] indicates that sediment settles significantly in the downstream part of the estuary during high flow discharge and low tide. Conversely, during low flow discharge and high tide, sediment tends to settle before reaching the estuary.

The transport of river bed particles by water currents is a primary focus in river hydrodynamics research [14]. Siltation caused by sedimentation is a significant issue in water resource management, particularly in rivers [15]. Numerical models of water that account for hydrodynamic processes are effective tools for understanding sediment transport mechanisms [16]. Research on sediment hydrology in the Palu River Estuary focuses on the sedimentation characteristics and sediment transport processes through 2D hydrodynamic numerical simulations.

1.1. Problem Statement

Understanding the transport and distribution of suspended sediments in water bodies is essential for mitigating the negative effects of sedimentation and coastal development. The movement of sediment grains in marine areas can be analyzed using theoretical and empirical methods developed in recent decades in open channel hydraulics, particularly for river flows and currents [17]. Sediment transport rates can be calculated using several methods, including the instantaneous method, the L.C. method, the Van Rijn method, the Meyer Peter Muller (MPM) method, the Einstein method, and the Frijlink method.

The hydrodynamics in the Palu River Estuary influence sedimentation, erosion, transportation, and material deposition processes. The interaction between water and solid particles is important in the sediment transport process. This interaction involves the exchange of momentum between the two and is influenced by flow turbulence. Flow turbulence arises from the shear stress generated by the kinetic energy of the moving fluid [18]. This will impact the physical condition of the estuary, geomorphological processes, and water quality, which will in turn affect the ecosystem in the Palu River estuary.

This study was conducted specifically after the disaster, without considering pre-disaster data, in order to assess the characteristics of sediment transport in the estuarine waters of the Palu River. It also examines how river flow and coastal dynamics in Palu Bay, with its distinct geological, hydrological, and hydrodynamic conditions, influence these characteristics. This research aims to quantitatively analyze the sedimentation results from each method, providing data-driven recommendations for sedimentation management [19], as well as identifying sediment transport patterns and analyzing the characteristics of suspended sediments and pollutant loads in the Palu River estuary. This study presents field data results in a hydrodynamic model and an empirical formula applicable to coastal area management and sedimentation mitigation. Modeling estuaries with similar geology is possible, but it is crucial to recognize that the hydrodynamic factors of each river influence the data generated.

2. Methods and Data Analysis

2.1. Methods

Data collection was conducted from May 5 to May 7, 2024, at 50 station points in the Palu River, Central Sulawesi, Sulawesi Island, Indonesia (Figure 1). Water samples were taken to test the concentration of Total Suspended Solids (TSS), and sediment samples bad load were collected to investigate the characteristics of the sediment. Water sampling was performed using a horizontal sampler at two different depths: 0 meters (surface) and 0.5 meters. The analysis of total suspended solids (TSS) in water and wastewater was conducted using the Indonesian National Standard method (SNI, 2004) through a gravimetric approach [20]. Basic sediment sampling was conducted using a grab sampler tool. Laboratory tests analyzing the sediment characteristics were carried out at the Soil Mechanics Laboratory, Faculty of Engineering, Hasanuddin University.

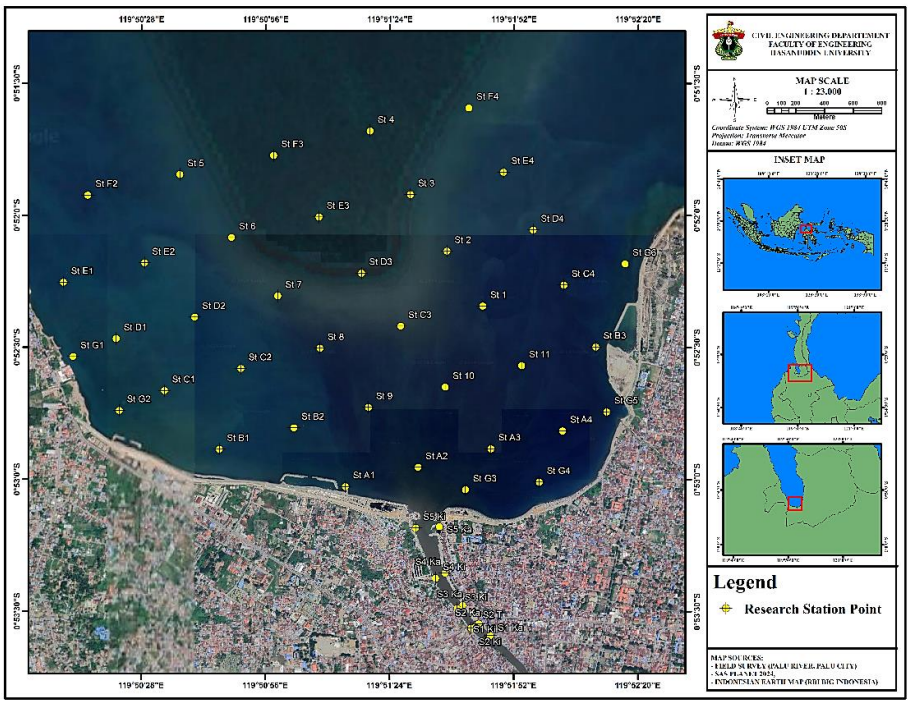

Figure 1. Research location map

Figure 2 shows the flowchart of the research methodology through which the objectives of this study were achieved.

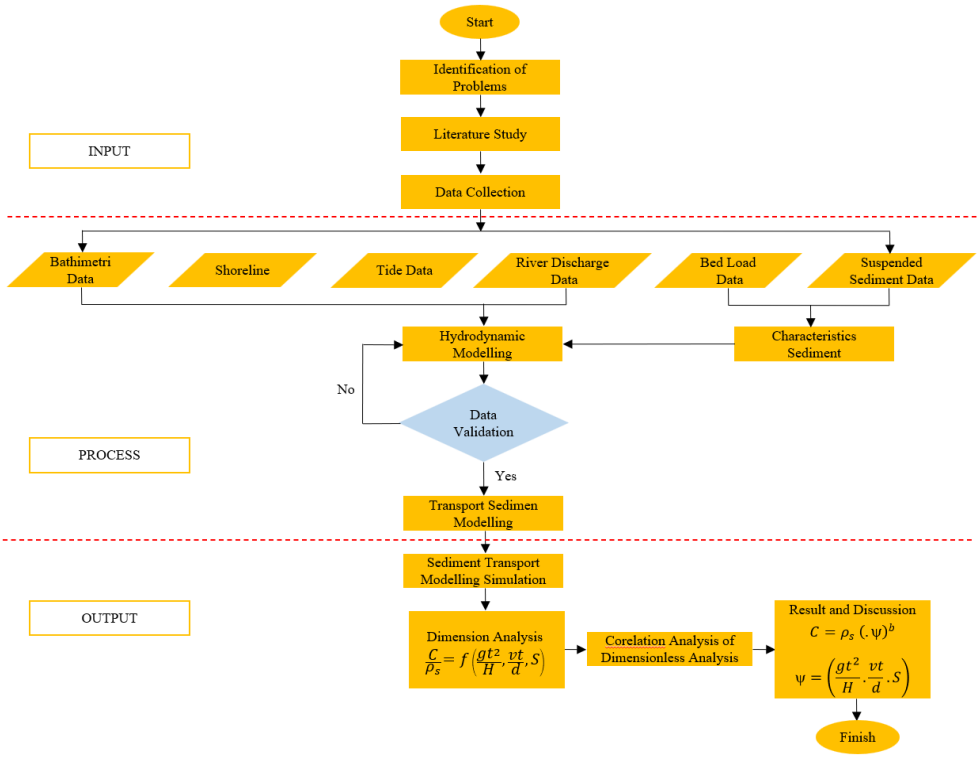

Figure 2. The flowchart of the experimental works

2.2. Data Analysis

The data analyzed consist of direct observations made at the research site, followed by laboratory analyses. These laboratory examinations are conducted to determine the size of sediment grains, their specific gravity, and sediment concentration. The characteristics of sediment can be described based on size, specific gravity, and fall velocity. Additionally, sediment particles are classified according to their type, size, and the mineral composition of the parent material, which may include gravel, sand, clay, and other materials. Based on their size, sediments can be classified as shown in Table 1.

Table 1. Type and size of particles

Type	Size Range (mm)
Gravel	2.0 – 20.0
Sand	0.063 – 2.0
Silt	0.0039 – 0.063
Clay	<0.0039

Specific gravity refers to the ratio between the weight of soil (Υ_s) and water (Υ_w) with equivalent contents as stated in the following Equation 1.

$$G_s = \frac{\Upsilon_s}{\Upsilon_w} \quad (1)$$

Apart from particle size, soil types can be classified based on respective specific gravity value, as shown in Table 2 and Figure 3.

Table 2. Specific Gravity Classification

Soil Type	G_s
Sand	2.65 – 2.68
Organic Silt	2.62 – 2.68
Organic Clay	2.58 – 2.65
Inorganic Clay	2.68 – 2.75
Peat	< 2

(a) (b)

Figure 3. Suspended sediment sample (a), Bed load sediment sample (b)

The fall velocity (w) is defined as the final velocity it takes sediment to settle, and can be calculated using the following Equation 2.

$$w = \left[\frac{gd^2}{18v}\right]\left(\frac{\rho_s - \rho_w}{\rho_w}\right) \quad (2)$$

where w is the falling speed, g is the acceleration due to gravity (9.81 m/s²), d is the particle size, ρ_s is the specific gravity of the particle, and ρ_w is the specific gravity of water.

Sediment transport calculations were performed using the Meyer-Peter Müller (MPM) method and the Frijlink method. The simulation of currents and sediment transport was conducted using the MIKE 21 Flexible Mesh (FM) Hydrodynamic (HD) module, MIKE 21 software with the Hydrodynamics module is used to create hydrodynamic models to understand current movement patterns based on the desired data [21], Additionally, the Sand Transport (ST) modules are used to model sediment transport. The data required include river discharge data, tides, bathymetry, current speed and direction, total suspended solids (TSS), and sediment grain size [22].

Sediment transport at the bottom of the channel is greatly influenced by the initial movement of particle grains when the critical stress is exceeded. However, the base material remained still or immobile, when the shear stress does not

exceed the critical stress value. The flow shear stress (r_0) is caused by the force of flow movement, known as the flow shear velocity ($\boldsymbol{u}_*$) expressed in the following Equation 3.

$$\mathrm{u} * = \sqrt{\mathrm{g} \,.\, \mathrm{R} \,.\, \mathrm{S}} \tag{3}$$

The flow shear stress (r_0) is expressed by the Equation 4.

$$r_0 = \rho_w \,.\, u_*^2 \tag{4}$$

The initial movement of sediment grains was influenced by the magnitude of the flow shear stress (r_0) occurring in the flow cross-section and critical shear stress (r_c)**.** Sediment particles tend to move assuming the

$r_0 < r_c$, then sediment grains are in a motionless or still condition,

$r_0 = r_c$, then the grains start moving,

$r_0 > r_c$, then sediment grains move.

The critical shear stress value (r_{c*}) is a comparison of the shear stress parameter (r_c) with the specific gravity (ρ_w) and grain diameter (D_s) as stated in the following Equation 5.

$$r_{c*} = \frac{r_c}{(\rho_s - \rho_w) D_s} \tag{5}$$

The value of the shear stress parameter (r_{c*}) was determined through the shields sediment particle movement diagram curve based on the Reynolds Number (*Re*). This number is a linear dimensionless factor with viscosity (u) expressed by the following Equation:

$$R_e = \frac{u_* . D_s}{u} \tag{6}$$

Sediment transport equation [23] is in line with the principle that movement depends on the existence of an energy slope. Sediment transport mass (g'_{sb}) and discharge equation (q_{sb}) are expressed in submerged weight per units (kg/s/m) Equation 7.

$$q_{sb} = \frac{g'_{sb}}{(\rho_s - \rho) \,.g} \tag{7}$$

Sediment transport equation [24] is based on statistical theory and the results of laboratory experimental observations, where the movement of particles at the bottom of the flow is caused by the presence of an uplift force greater than the weight or mass in water. The bottom sediment transport discharge (q_b) is stated in Equation 8.

$$q_b = \Phi * x \sqrt{\left(\frac{\rho_S - \rho_w}{\rho_w}\right) \times g \times D_{50}} \times \rho_s \tag{8}$$

Sediment transport intensity parameter ($\Phi*$) was determined based on the value of the flow intensity or shear stress (ψ_*). This is denoted in the relationship curve between sediment transport intensity ($\Phi*$) and flow intensity or shear stress (ψ_*) in Figure 4. The value of the flow intensity was calculated using Equation 9.

$$\psi * = \frac{(\rho_S - \rho_w)}{\rho_w} \cdot \frac{d}{R_h \,.\, \mu \,.\, S} \tag{9}$$

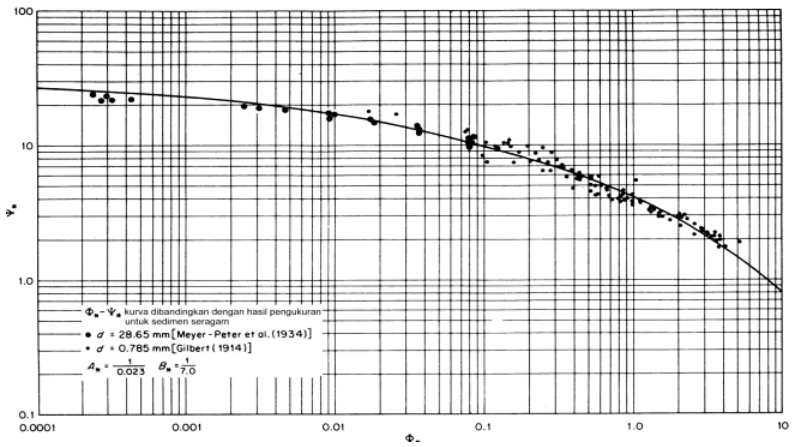

Figure 4. Sediment transport parameter graph

Equation Frijlink [25] was used to calculate the quantity of bed sediment transport (bed load) as stated in Equation 10.

$$\Phi * = \frac{q_{sb}}{d_m \sqrt{g \,.\, R_h \,.\, \mu \,.S_0}} = 5 \exp\left[-0{,}27 \frac{(\rho_S - \rho_w)}{\rho_w} \,.\, \frac{d_m}{R_h \,.\, \mu \,.\, S_0}\right] \quad (10)$$

Where, $\Phi *$ is sediment transport intensity that has an empirical relationship with the flow intensity or shear stress (ψ') stated in Equation 11.

$$\psi * = \frac{(\rho_S - \rho_w)\, d_{50}}{R_h \,.\mu \,.\, S_0} \quad (11)$$

The basic channel condition parameter (μ) is expressed as the ratio of the basic roughness to sediment grain particles, stated in Equation 12.

$$\mu = \left(\frac{C}{C_{d90}}\right)^{3/2} \quad (12)$$

The values of the basic roughness (C) and friction factor (C_{d90}) were determined using the Chezy Equation stated in 13 and 14.

$$C = 18 log \frac{12h}{k} \quad (13)$$

$$C_{d90} = 18 log \frac{12h}{d_{90}} \quad (14)$$

The hydraulic roughness of the channel (k) was determined by using Equation 15.

$$u_z = 5.75\, u_* \, log \frac{33h}{k_s} \quad (15)$$

The quantity of bed load sediment transport was calculated using the following empirical methods stated in the MPM, Einstein, and Frijlink equations. Additionally, these three equations served as a basis for predicting the extent of sediment transport discharge in respect to the cross-section of the points reviewed in the Palu River.

The HD model was generated using the continuity Equation, and mass momentum on the x and y axes [26].

Continuity Equation:

$$\frac{\partial \varsigma}{\partial t} + \frac{\partial p}{\partial x} + \frac{\partial p}{\partial y} = \frac{\partial d}{\partial t} \quad (16)$$

Mass momentum about the x-axis:

$$\frac{\partial p}{\partial t} + \frac{\partial}{\partial x}\left(\frac{p^2}{h}\right) + \frac{\partial}{\partial y}\left(\frac{pq}{h}\right) + gh\left(\frac{\partial \varsigma}{\partial x}\right) + \frac{gp\sqrt{p^2+q^2}}{C^2.h^2} - \frac{1}{\rho w}\left[\frac{\partial}{\partial x}(h\tau_{xx}) + \frac{\partial y}{\partial y}\left(h\tau_{xy}\right)\right] - \boldsymbol{\Omega} q - fVV_x + \frac{h}{\rho w}\frac{\partial}{\partial x}(p_a) = 0 \quad (17)$$

Mass momentum about the y-axis:

$$\frac{\partial p}{\partial t} + \frac{\partial}{\partial y}\left(\frac{q^2}{h}\right) + \frac{\partial}{\partial x}\left(\frac{pq}{h}\right) + gh\left(\frac{\partial \varsigma}{\partial y}\right) + \frac{gp\sqrt{p^2+q^2}}{C^2.h^2} - \frac{1}{\rho w}\left[\frac{\partial}{\partial y}\left(h\tau_{yy}\right) + \frac{\partial y}{\partial y}\left(h\tau_{xy}\right)\right] - \boldsymbol{\Omega} q - fVV_y + \frac{h}{\rho w}\frac{\partial}{\partial y}(p_a) = 0 \quad (18)$$

The following equations were used to obtain sediment transport (ST) module, the Engelund-Hansen, Van-Rijn, Englund-Fredsoe, and Meyer-Peter-Muller models [20].

$$\frac{\partial z}{\partial t} = \frac{z\,(1+a-e^z)}{e^z(z-1)+1}\left(\frac{1}{U_0}\right)\left(\frac{dU_0}{dt}\right) + \frac{30K}{k}\left(\frac{\sqrt{K^2{U_0}^2 + z^2{U_{f0}}^2 + 2Kz\, U_{f0}\, U_0\, cosy}}{e^z(z-1)+1}\right) \quad (19)$$

where (K) is the Von Karman constant, (t) time, (z) boundary layer thickness parameter, (U_0) nearest wave base orbital velocity, (U_{f0}) the current shear velocity in the wave boundary layer, (γ) the angle between the current and the wave, (k) the surface roughness of the base 2.5 d50 and 2.5 d50 + kg for plane and ripple covered beds, respectively (d50) the average diameter size, while (k_R) is the ripple related to roughness.

The vertical sediment transport value in the sand module was calculated using the diffusion equation, stated as follows:

$$\frac{\partial c}{\partial t} = w\frac{\partial c}{\partial y} + \frac{\partial}{\partial y}\left(\varepsilon_s \frac{\partial c}{\partial y}\right) \quad (20)$$

where (ε_s) is the turbulence coefficient, (c) suspended sediment concentration, and (w) vertical velocity.

3. Analysis Results

3.1. Distribution of Total Suspended Solids (TSS)

The results of laboratory analysis showed that TSS concentrations around the Palu River estuary varied. At a depth of 0.0 m, TSS concentrations ranged from 0.018 to 1.540 g/L with an average of 0.239 g/L. At a depth of 0.5 m, TSS values ranged from 0.026 to 1.370 g/L, with an average of 0.264 g/L. The higher TSS concentration at a depth of 0.0 m indicates that most of the suspended solids originate from land erosion and are carried by water flow from both rivers and the sea (Figure 5). This suggests that erosion activities around the estuary significantly contribute to the increase in TSS [27].

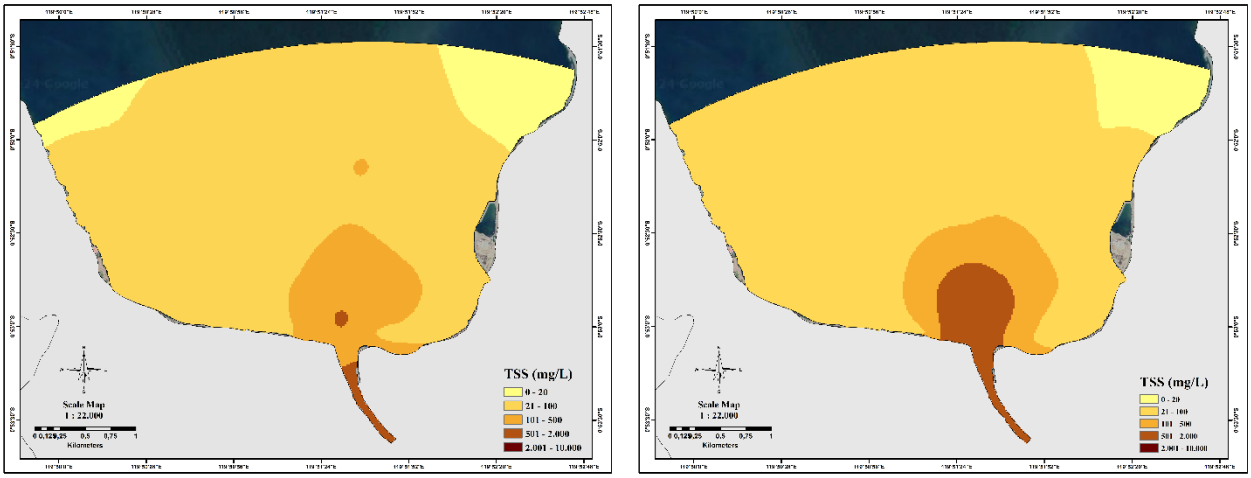

(a) (b)

Figure 5. (a) Distribution Condition of TSS Depth 0.0 m, (b) Distribution Condition of TSS Depth 0.5 m

3.2. Sediment Characteristics

Based on the results of the analysis of bad load sediments in the Palu River (Table 3), the types of sediments at the research site are silt, silty sand, and sand, with a dominance of silty sand. The sediment becomes finer towards the estuary. This distribution occurs because currents play a crucial role in transporting sediment, moving it along with the energy they possess. The distribution of sediment composition at the study site is shown in Figure 6.

Table 3. Analysis of Bad Load Sediment in Palu River

Station Point	Content (%)				Sediment Types
	Gravel	Sand	Silt	Clay	
S1 Ka	0.00	76.00	24.00	0.00	Silty Sand
S1 Ki	0.67	60.67	38.67	0.00	Silty Sand
S2 ka	0.40	87.40	12.20	0.00	Silty Sand
S2 T	3.33	72.33	24.33	0.00	Silty Sand
S2 Ki	5.67	50.33	44.00	0.00	Silty Sand
S3 ka	4.20	90.80	5.00	0.00	Sand
S3 ki	4.80	74.00	21.20	0.00	Silty Sand
S4 ka	0.60	73.60	25.80	0.00	Silty Sand
S4 ki	1.60	94.20	4.20	0.00	Sand
S5 ka	0.20	87.80	12.00	0.00	Silty Sand
S5 ki	0.67	29.67	47.24	22.43	Silt
S6 ka	0.40	66.40	33.20	0.00	Silty Sand
S6 T	0.00	78.20	21.80	0.00	Silty Sand
S6 ki	0.00	51.33	35.90	12.77	Silty Sand

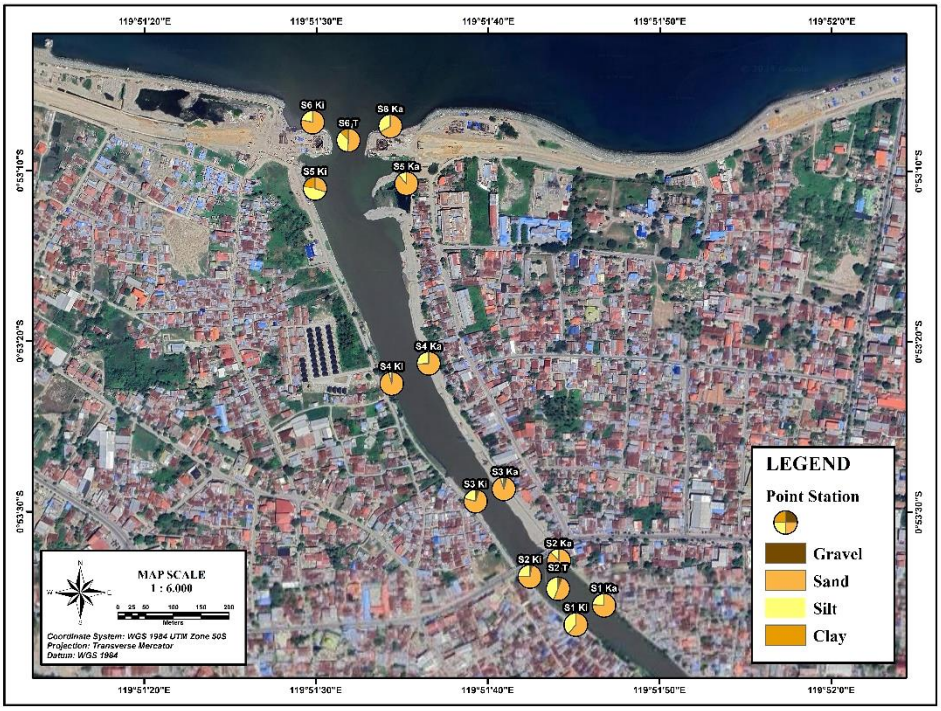

Figure 6. Distribution Map of Composition of Bad Load Sediment Content in the Palu River

The results of sediment grain gradation analysis showed that the organic silt soil type constituting the bottom sediment have a specific gravity (G_s) ranging from 2.64 to 2.69 **(**kg/m^3), and are mainly dominated by sand. Additionally, sediment particle gradation with grain size D_{50} and D_{90} ranged from 0,101 mm to 4.358 mm and 0.221 mm to 14.946 mm, respectively (Table 4).

This variation in grain size indicates the influence of river currents on sediment movement, where stronger currents can transport larger sediments. This particle size distribution is important for understanding the sedimentation process and its impact on the ecosystem.

Table 4. Laboratory Analysis Results of Specific Gravity and Sediment Grain Size Diameter

Station	Specific gravity (G_s) (kg/m^3)	Soil Type	Sediment Grain Size Diameter			
			d_{50} (mm)	d_{50} (m)	d_{90} (mm)	d_{90} (m)
S6 Ki	2.67	Sand	0.266	0.00027	3.528	0.00353
S6 Ka	2.65	Sand	0.535	0.00054	4.400	0.00440
S5 Ki	2.67	Sand	0.111	0.00011	0.358	0.00036
S5 Ka	2.68	Sand	0.171	0.00017	0.385	0.00039
S4 Ki	2.69	Sand	3.234	0.00323	8.702	0.00870
S4 Ka	2.64	Organic Silt	4.358	0.00436	8.456	0.00846
S2 Ki	2.69	Sand	0.101	0.00010	0.221	0.00022
S2 Ka	2.66	Sand	2.647	0.00265	14.946	0.01495
S1 Ki	2.68	Sand	2.716	0.00272	12.008	0.01201
S1 Ka	2.69	Sand	2.822	0.00282	8.776	0.00878

3.3. HD Simulation and Sediment Transport

The results of the HD simulation produced a picture related to the current pattern observed at the highest, towards low, and high tides, including the lowest ebb as shown in Figure 7. In general, the model showed a uniform current migrating towards river mouth due to the high discharge of 96,073 m^3/s in the Palu River.

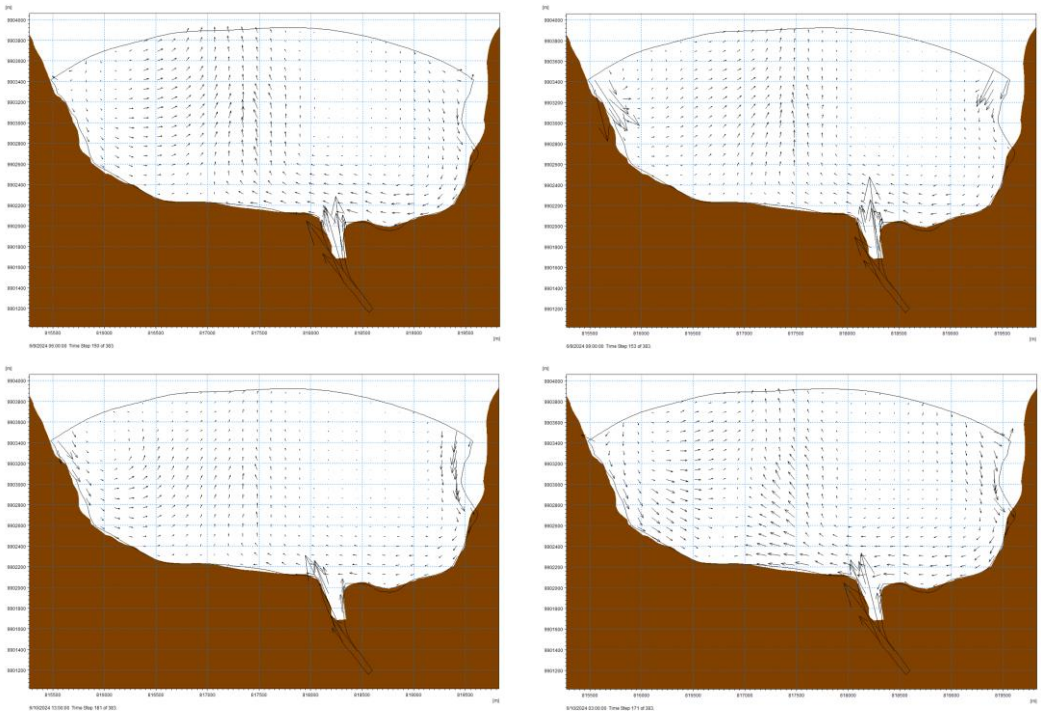

Figure 7. Current patterns at high tide, towards low tide, lowest ebb, and towards high tide

Based on the results of sediment transport simulations, an increase in sediment concentration was observed towards the low tide and lowest ebb, alongside the flow towards river mouth. However, a decrease was observed towards the high and highest tides, as shown in Figure 8.

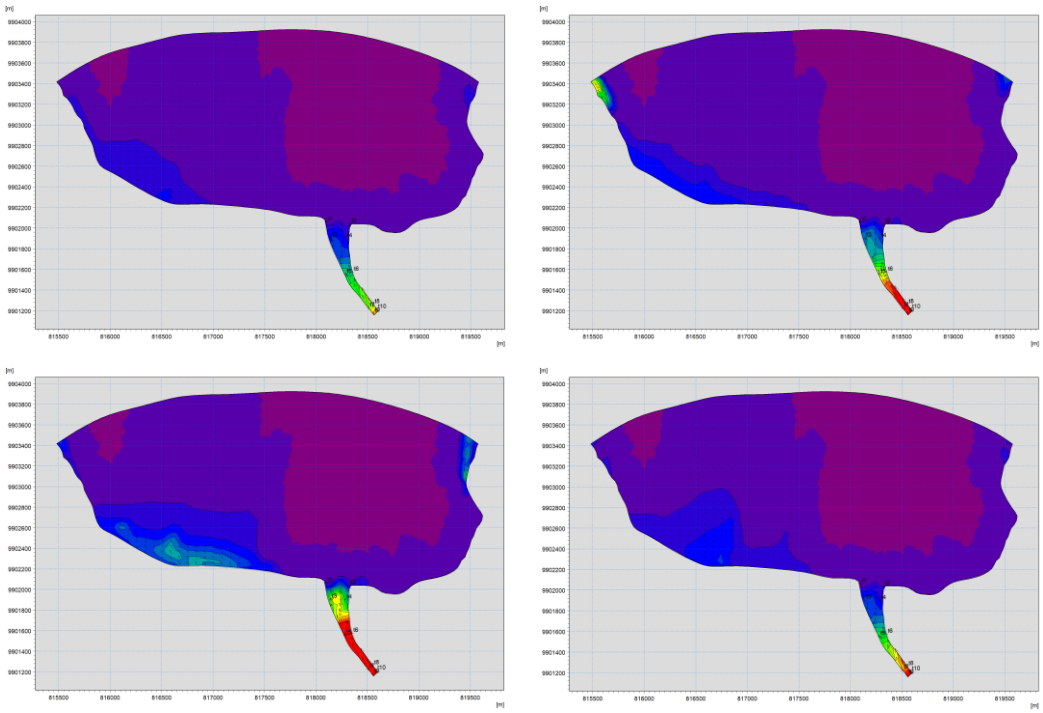

Figure 8. Sediment transport patterns at high tide, towards low tide, lowest ebb, and towards high tide

3.4. Bed Sediment Transport Discharge

The profile and cross-sectional data of the Palu River channel describe the dimensions of the flow profile and cross-sectional dimensions of the channel at each measurement station location. The cross-section of the river flow channel under review and the cross-sectional dimension profile at each station can be seen in Table 5. According to the table, the highest discharge value (Q) was obtained at the S6 Ki - S6 Ka cross-section, with a value of 40.357 m^3/s, and the lowest at the S2 Ki - S2 Ka cross-section, with a discharge value of 20.085 m^3/s.

Table 5. Cross-section profile data and results of Palu River discharge calculations

Cross section	Average speed (V); m/s	Cross-sectional area (A); m^2	Channel base slope (I)	Water depth (h); m	Base width (b); m	Wet circumference (P); m	Hydraulic radius (R); m	Grain shear velocity (U*); m/s	y	Base width (b)	Discharge (Q); m^3/s
S6 Ki – S6 Ka	1.579	39.281	0.002	1.606	7.963	11.180	1.158	0.146	4.762	7.963	40.537
S5 Ki – S5 Ka	1.865	21.803	0.002	1.543	5.790	8.892	1.032	0.138	3.548	5.790	23.088
S4 Ki – S4 Ka	2.103	27.451	0.002	1.667	6.219	9.600	1.129	0.144	3.981	6.219	34.977
S2 Ki – S2 Ka	2.161	15.076	0.002	1.237	4.874	7.356	0.836	0.124	2.950	4.874	20.085
S1 Ki – S1 Ka	1.829	24.349	0.002	1.556	5.444	8.676	1.055	0.139	3.749	5.444	31.702

The stability control analysis of the basic grain particles in Table 6, showed that the value of the flow shear stress (τ_0) at each station reviewed was greater than the critical shear stress (τ_c). This implied that the occurrence of sediment transport at each station led to the erosion at the bottom of river.

Table 6. Stability control of basic granular particles

Station	u* (m/s)	t_o	t_{c*}	Stability control	
S6 Ki	0.172	21.24	0.17	$\tau_0 > \tau_c$	Moving Particles / Erodible Bed
S6 Ka	0.172	21.24	0.29	$\tau_0 > \tau_c$	Moving Particles / Erodible Bed
S5 Ki	0.168	19.37	0.11	$\tau_0 > \tau_c$	Moving Particles / Erodible Bed
S5 Ka	0.168	19.37	0.11	$\tau_0 > \tau_c$	Moving Particles / Erodible Bed
S4 Ki	0.175	20.90	9.65	$\tau_0 > \tau_c$	Moving Particles / Erodible Bed
S4 Ka	0.175	20.90	11.92	$\tau_0 > \tau_c$	Moving Particles / Erodible Bed
S2 Ki	0.151	15.67	0.10	$\tau_0 > \tau_c$	Moving Particles / Erodible Bed
S2 Ka	0.151	15.67	12.07	$\tau_0 > \tau_c$	Moving Particles / Erodible Bed
S1 Ki	0.169	19.27	11.64	$\tau_0 > \tau_c$	Moving Particles / Erodible Bed
S1 Ka	0.169	19.27	11.23	$\tau_0 > \tau_c$	Moving Particles / Erodible Bed

Sediment transport discharge was calculated using the Meyer-Peter Müller (MPM) and Frijlink equations. Based on calculations using these equations (Table 7), the resulting sediment transport discharge varies. The sediment transport discharge calculation results are expressed in units of sediment particle transport discharge at each station under review. The results of the sediment transport discharge calculations from each equation are then used to interpret the value of sediment transport discharge occurring in the Palu River. Based on the analysis of sediment transport for each location point reviewed using two equations, the results of the sediment transport discharge value (q_b) varied, with the largest values occurring at point 9 (MP-M and Frijlink) with values of 47.61 m^3/day and 72.94 m^3/day, respectively. Based on the sediment transport values, it can be estimated that the potential sedimentation occurring in the downstream area is 72.94 m^3/day. The variation in sediment transport discharge values at each location point is strongly influenced by flow characteristics, channel geometry, and basic sediment grain size.

Table 7. The results of the analysis of bed load field discharge with model results at each station.

Station	Reynold Number (*Re*)	Froude Number (*Fr*)	Channel Roughness Height(k) (m)	Basic Roughness Coefficient (C) ($m^{1/2}/s$)	Basic Roughness Coefficient Ratio(μ)	Sediment Transport Discharge (Qb) (m^3/hr)		ST Simulation Model Results
						MPM	Frijlink	
S6 Ki	0.046	0.79	0.42	0.42	0.54	39.72	11.97	0.39
S6 Ka	0.092	0.79	0.44	0.44	0.56	41.62	22.64	0.48
S5 Ki	0.019	0.61	0.31	0.31	0.41	9.43	3.07	2.58
S5 Ka	0.029	0.61	0.32	0.32	0.42	9.41	4.51	2.08
S4 Ki	0.566	0.79	0.68	0.68	0.71	38.28	65.68	5.22
S4 Ka	0.762	0.79	0.78	0.78	0.78	35.08	65.20	5.02
S2 Ki	0.015	0.77	0.39	0.39	0.52	12.60	3.15	4.90
S2 Ka	0.399	0.77	0.58	0.58	0.64	30.77	52.11	5.28
S1 Ki	0.459	0.83	0.65	0.65	0.71	47.61	72.94	6.00
S1 Ka	0.477	0.83	0.65	0.65	0.71	41.86	67.34	7.38

The relationship between the Froude number (Fr) and sediment transport discharge (qb) is illustrated in the curve presented in Figure 9. The logarithmic curve that connects the Froude number (Fr) with sediment transport discharge represents an interpretation of the sediment transport characteristics occurring at the Palu River cross-section point. An excessive rate of sediment transport can lead to issues such as reducing the flow capacity of the river at river or irrigation structures, hampering their operation, and reducing storage capacity.

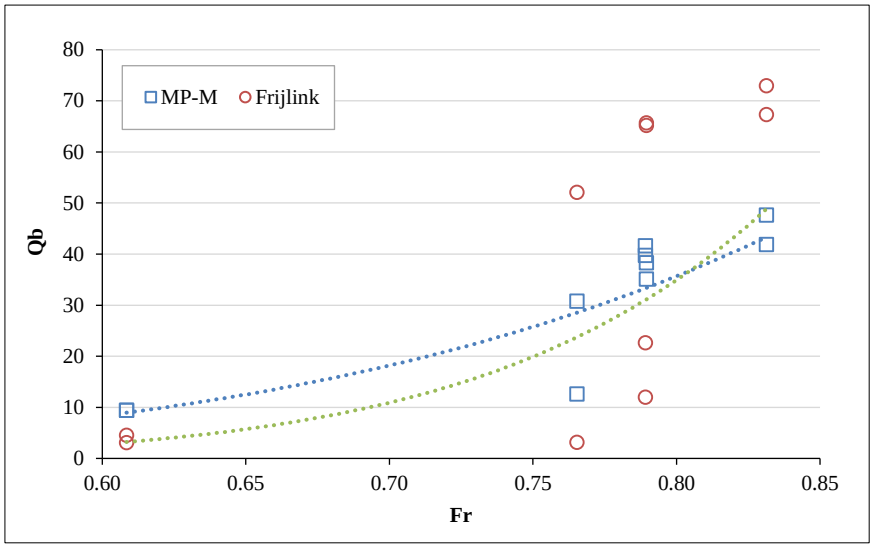

Figure 9. The relationship between sediment transport discharge (qb) and the Froude number (Fr)

Based on the simulation results using the Sand Transport (ST) module, the values of sediment transport discharge at each point were analyzed. The results show fluctuations in sediment transport discharge on both the right and left sides of the river. The concentration of sediment transport discharge in the upstream part decreases towards the downstream or estuary (Table 7), with the highest value at point S1 Ka of 7.38 m³/hr and the lowest at point S6 Ki of 0.39 m³/hr.

The relationship between sediment transport discharge (Qb) from the simulation model and the field results (MPM and Frijlink calculations) are represented by the curve shown in Figure 10. The curve shows that the relationship between the simulation model and Frijlink calculations had a larger R^2 value compared to the MP-M of 0.4435.

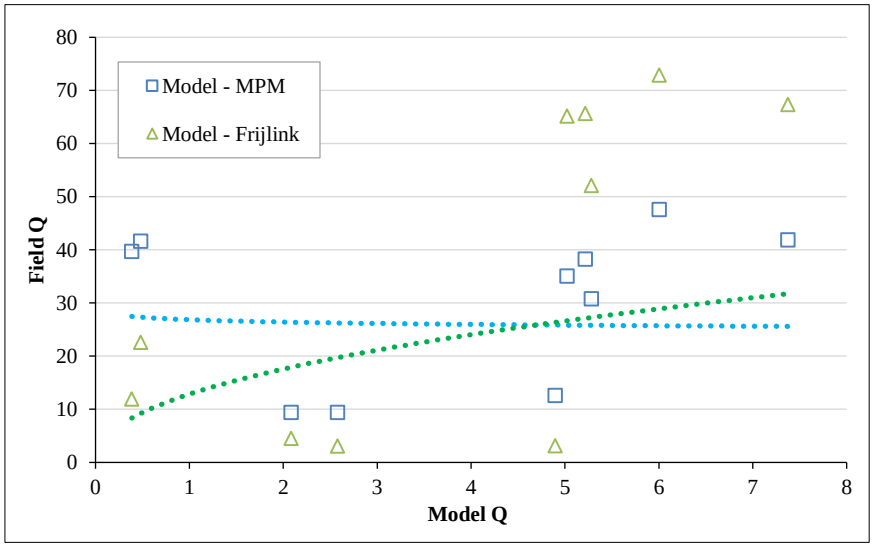

Figure 10. The relationship between sediment transport discharge (Qb) from simulation models and field results

The results of the analysis produced a dimensionless relationship between several parameters estimated to influence sediment concentration.

$$C = f\left(d, H, v, t, \rho_s, \rho_w, g, S\right) \tag{21}$$

where C is sediment concentration (mg/l), d flow depth (m), H tidal height (m), v tidal current velocity (m/s), t tidal time (s), ρ_s sediment density (kg/m^3), ρ_w water density (kg/m^3), g gravitational acceleration (m/s^2), and S salinity (-).

$$\frac{C}{\rho_s} = f\left(\frac{gt^2}{H}, \frac{vt}{d}, S\right) \quad (22)$$

The non-dimensional form stated in Equation 22, was used to analyze the interaction between these parameters by eliminating respective units, enabling a general interpretation across scales and conditions. In addition, $\frac{C}{\rho_s}$ represents the dimensionless sediment concentration normalized by the density. $\frac{gt^2}{H}$ is a dimensionless parameter that shows the relationship between gravity and tidal height. This parameter shows the influence of gravitational deposition over time on tidal height. $\frac{vt}{d}$ is a ratio that represents the relationship between tidal velocity and water depth. The intensity of the flow compared to the water depth, affects sediment suspension and transport, with S a dimensionless parameter, representing salinity.

This form helped in understanding how changes in the factors impacted sediment concentration in a simplified and comparable manner, regardless of the specific units or scales of the original parameters. It made provisions for the comparison of results obtained from previous research and geographic locations by focusing on the underlying relationships between variables. Correlation analysis was used to analyze dimensionless relationships, including obtain constants and coefficients in line with the resulting sediment concentration parameter (C/ρ_s).

The graph shows a dimensionless relationship, and the empirical equation used to obtain sediment concentration

$$C = \rho_s(a.\psi)^b, \quad (23)$$

with coefficient value a = 412.71 and b = (-0.545) where $\psi = \left(\frac{gt^2}{H}.\frac{vt}{d}.S\right)$.

4. Discussion

4.1. Distribution of Total Suspended Solid (TSS)

The concentration and distribution distance of suspended sediment in the sea are influenced by several factors, such as river discharge, the concentration of suspended sediment from the river, the diffusion coefficient, and ocean currents. These factors move the mass of water along with suspended sediments when sediment transport reaches the sea. Based on the distribution of TSS concentrations at depths of 0 and 0.5 m (Figure 5), the concentration increases from the river towards the mouth and decreases as it gets further from the mouth towards the sea. This condition can cause siltation in the bends of the river, the estuary, and the bay around the estuary. This is supported by previous research, which states that the high discharge of the Palu River causes siltation not only in the river body but also in the estuary and Palu Bay. At the lowest ebb, it can be seen that the land at the mouth of the river is slightly to the west.

4.2. Sediment Transport Discharge

The particle stability control analysis results show that the flow shear stress value ($\boldsymbol{\tau_0}$) at each station is greater than the critical shear stress value ($\boldsymbol{\tau}$c). This indicates that sediment transport occurred at all stations studied, contributing to the erosion of the Palu River bed. This finding is important for understanding how sediments move and potentially cause morphological changes along the river. By comparing the Froude number (Fr) to the sediment transport discharge (qb) as expressed by their relationship curve, the characteristics of sediment transport in the Palu River were obtained. The relationship curve indicates that an increase in the Froude number (Fr) at each cross-sectional section is directly proportional to an increase in sediment transport discharge (qb). Thus, using the graph of the relationship between the Froude number (Fr) and sediment transport discharge (qb), the characteristics of sediment transport at the station points of the Palu River section can be identified.

"The relationship between tidal parameters and sediment concentration can be seen in Figure 11-a. Figure 11-a shows that each additional tidal value increases the sediment concentration. Similarly, the relationship between the depth parameter and sediment concentration can be seen in Figure 11-b. Figure 11-b illustrates that every additional depth value also increases the sediment concentration.

Figure 12-a shows the relationship between the salinity parameter and sediment concentration, where an increase in salinity results in a decrease in sediment concentration. This observation aligns with field observations, which indicate higher sediment concentrations in areas with low salinity. Figure 12-b illustrates the relationship between the parameter combination ψ and sediment concentration. The value of ψ increases as sediment density decreases, demonstrating how the dimensionless parameter ψ relates to sediment concentration normalized by sediment density. As ψ increases, factors such as increased tidal timing, higher velocities, greater salinity, or decreased tidal height and depth influence sediment dynamics. An increase in ψ suggests that the energy available in the system is more effective in dispersing or transporting sediment, reducing its local concentration. Essentially, higher tidal velocity or timing leads to more significant sediment dispersal, preventing accumulation in a single location.

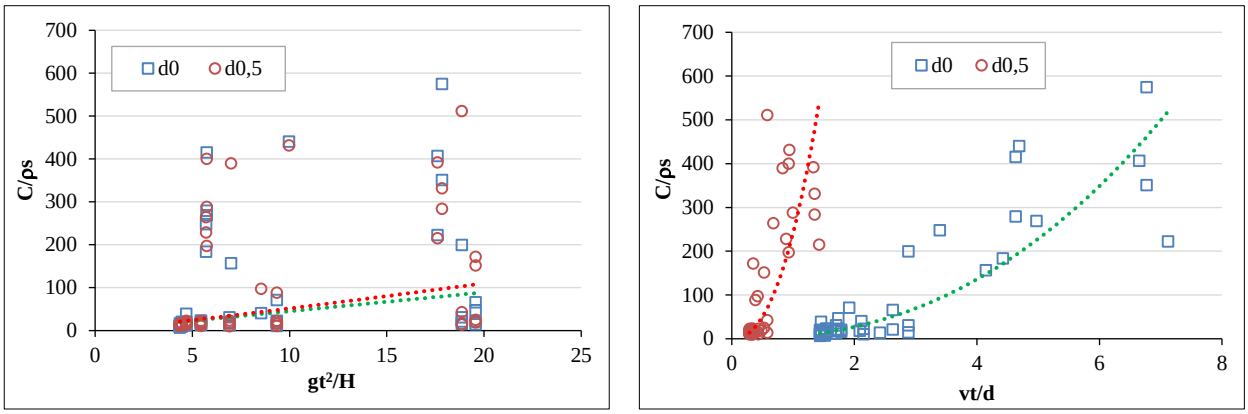

(a) (b)

Figure 11. (a) The relationship between tidal parameters and sediment concentration, (b) The relationship between depth parameters and sediment concentration

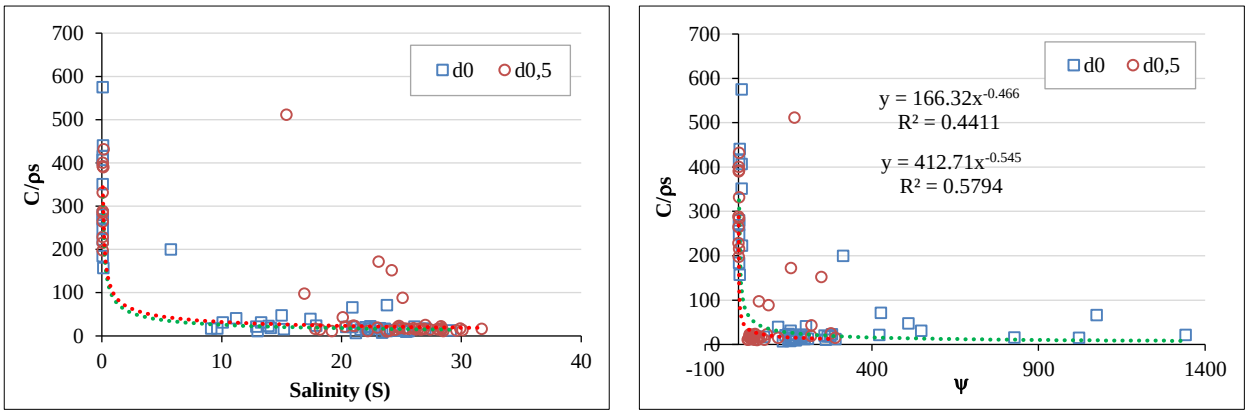

(a) (b)

Figure 12. (a) The relationship between salinity parameters and sediment concentration, (b) The relationship between combination parameters and sediment concentration

When current velocity (v) or tidal time (t) increases, or when depth (d) decreases, these conditions favor increased turbulence and stronger current forces, leading to sediment being transported away from its source rather than settling. This reduces the local concentration of suspended sediments. Salinity (S) can also influence sediment settling behavior, as higher salinity increases water density. This can promote either suspension or settling, depending on the interaction of other forces such as velocity, turbulence, buoyancy, particle properties, and gravity.

The relationship between ψ and sediment concentration ($C/\rho s$) shows that as the energy imparted by water motion increases (through greater velocity or longer duration), sediment becomes more dispersed, leading to a decrease in its local concentration. High-energy dynamic conditions tend to distribute sediment more evenly, thus reducing sediment concentrations in specific areas.

4.3. Hydrodynamics Simulation and Sediment Transport

The pattern suggests that during periods of high flow, there is potential for greater sedimentation in the estuary, which can affect water quality and ecosystems. The confluence of tidal currents from the sea and river currents at high tide and just before high tide causes a reduction in flow velocity in the Palu River estuary. During these conditions, the currents around the coast and estuary are weakened due to the movement of water masses as sea levels rise, causing seawater to move towards lower elevations and dominate the coastal area. Conversely, at low tide and just before low tide, there is an increase in flow in the river body, especially in the river bend area towards the estuary. When the tide enters the river, it behaves like a wave that rises upstream, becomes distorted, and eventually dissipates due to the friction of the river bed and flow [28]. The current movement in each condition exhibits differences in direction and deflection after the tidal current reaches its minimum and maximum.

Sediment concentration in each condition will always fluctuate, although slightly. During the conditions leading to the lowest ebb and low tide, there is an increase in sediment concentration along the river flow towards the estuary. Conversely, during the conditions leading to the highest tide and high tide, there is a decrease in sediment concentration. This fluctuation occurs because sediment transport is influenced by currents that move and settle sediment material.

Simulation results indicate that areas of the river flow with greater current speed will transport more sediment. When the current speed decreases, larger sediment particles begin to settle and accumulate at the bottom. The interaction between turbulence and sediment distribution can accurately predict sediment transport in coastal environments [29]. This study shows that there is a pattern of sediment dispersal and accumulation that occurs periodically. When the tidal current carries sediment to the estuary, there is a buildup of sediment in the lower reaches of the river. At low tide, the river flow velocity transports the sediment accumulated in the lower reaches to the western part of the estuary.

5. Conclusion

The concentration of suspended solids (TSS) in the Palu River was high, with concentrations increasing towards the estuary and decreasing as they moved away from the sea, at both 0 m and 0.5 m depths. Sediment characteristics at the study site showed variations, with a dominance of sandy to gravelly sand. Simulation results show that higher current velocities contribute to greater sediment transport. Conversely, as the current speed decreases, larger sediment particles begin to settle at the bottom of the water. The current pattern also affects the distribution of suspended sediment. During conditions leading to the lowest ebb and low tide, there is an increase in sediment concentration along the river flow towards the estuary. However, during conditions leading to the highest tide and high tide, there is a decrease in sediment concentration.

The results were stated in the correlation equation showing the relationship between dimensionless parameters, namely $C = \rho_s.(a.\psi)^b$ with coefficient value a = 412.71 and b = (-0.545) where $\psi = \left(\frac{gt^2}{H}.\frac{vt}{d}.S\right)$. The relationship between ψ and sediment concentration (C/ρ_s) shows that as the energy imparted by water motion increases (through greater velocity or longer duration), sediment becomes more dispersed, leading to a decrease in its local concentration. High-energy dynamic conditions tend to distribute sediment more evenly, reducing sediment concentrations in the estuarine region. These results help in understanding the dynamics of sediment transport in coastal and estuarine environments, particularly in predicting how sediment concentrations will change in response to different environmental conditions.

Recommendations for coastal management; this research provides locally specific data that can be used for coastal area management and mitigation of sedimentation issues. These data-driven recommendations are important for maintaining the stability of coastal ecosystems and reducing the negative impacts of sedimentation.

6. Declarations

6.1. Author Contributions

Conceptualization, A.S., M.A.T., M.P.H., and F.M.; methodology, M.A.T., M.P.H., and F.M.; validation A.S., M.A.T., M.P.H., and F.M.; formal analysis, A.S.; investigation, A.S.; resources, A.S.; data curation, A.S.; writing—original draft preparation, A.S.; writing—review and editing, A.S., M.A.T., M.P.H., and F.M.; visualization, A.S.; supervision, M.A.T., M.P.H., and F.M.; project administration, A.S.; funding acquisition, A.S. All authors have read and agreed to the published version of the manuscript.

6.2. Data Availability Statement

The data presented in this study are available on request from the corresponding author.

6.3. Funding

The authors received no financial support for the research, authorship, and/or publication of this article.

6.4. Conflicts of Interest

The authors declare no conflict of interest.

7. References

[1] Rusdin, A., Oshikawa, H., Divanesia, A. M. A., & Hatta, M. P. (2024). Analysis and Prediction of Tidal Measurement Data from Temporary Stations using the Least Squares Method. Civil Engineering Journal (Iran), 10(2), 384–403. doi:10.28991/CEJ-2024-010-02-03.

[2] Arianty, N., Mudin, Y., & Rahman, A. (2017). Wave refraction modeling and analysis of ocean wave characteristics in Palu Bay waters. Gravitasi, 16(2), 23-30. doi:10.22487/gravitasi.v16i2.9474. (In Indonesian).

[3] Matos, T., Martins, M. S., Henriques, R., & Goncalves, L. M. (2024). Design of a sensor to estimate suspended sediment transport in situ using the measurements of water velocity, suspended sediment concentration and depth. Journal of Environmental Management, 365, 121660. doi:10.1016/j.jenvman.2024.121660.

[4] Sembiring, A. E., Mananoma, T., Halim, F., & Wuisan, E. M. (2014). Sedimentation Analysis in Panasen River Estuary. Jurnal Sipil Statik, 2(3), 148-154. (In Indonesian).

[5] Zhang, L., Guan, J., Zhong, D., & Wang, Y. (2023). Effect of sediment particles on the velocity profile of sediment–water mixtures in open-channel flow. International Journal of Sediment Research, 38(3), 361-373. doi:10.1016/j.ijsrc.2022.11.005.

[6] Li, Z., Chen, S., Sun, B., Wang, F., Zhang, L., & Wang, B. (2024). The characteristics of water and sediment movement in the confluence area of pipeline. Urban Water Journal, 21(8), 927-940. doi:10.1080/1573062X.2024.2397787.

[7] Hatta, M. P., Widyastuti, I., & Makkarumpa, A. M. M. (2023). The Effect of Triangle Slope Variation on Froude Number with Numerical Simulation. Civil Engineering Journal (Iran), 9(12), 3136–3146. doi:10.28991/CEJ-2023-09-12-012.

[8] Damseth, S., Thakur, K., Kumar, R., Kumar, S., Mahajan, D., Kumari, H., ... & Sharma, A. K. (2024). Assessing the impacts of riverbed mining on aquatic ecosystems: A critical review of effects on water quality and biodiversity. HydroResearch, 7, 122-30. doi:10.1016/j.hydres.2024.01.004.

[9] Karamma, R., Pallu, M. S., Thaha, M. A., & Hatta, M. P. (2020). A 2nd numerical model of salinity distribution pattern on the estuary of Jeneberang River. IALT, 22(March), 192–200.

[10] Garres-Díaz, J., Fernández-Nieto, E. D., & Narbona-Reina, G. (2022). A semi-implicit approach for sediment transport models with gravitational effects. Applied Mathematics and Computation, 421, 126938. doi:10.1016/j.amc.2022.126938.

[11] Setiawan, I., Haditiar, Y., Syukri, M., Ismail, N., & Rizal, S. (2023). Suspended sediment transport generated by non-hydrostatic hydrodynamics in Northern Waters of Aceh, Indonesia. Heliyon, 9(6), e17367. doi:10.1016/j.heliyon.2023.e17367.

[12] Bilotta, G. S., & Brazier, R. E. (2008). Understanding the influence of suspended solids on water quality and aquatic biota. Water Research, 42(12), 2849–2861. doi:10.1016/j.watres.2008.03.018.

[13] Herman, R., Tanga, A., Tunas, I. G., Ishak, M. G., & Madman, A. (2022). Characteristics of Sediment Transport after Morphological Changes at Palu Estuary, Sulawesi, Indonesia as the Impact of 2018 Tsunami. International Journal of Integrated Engineering, 14(9), 8–14. doi:10.30880/ijie.2022.14.09.002.

[14] Chen, X., Chen, L., Stone, M. C., & Acharya, K. (2020). Assessing connectivity between the river channel and floodplains during high flows using hydrodynamic modeling and particle tracking analysis. Journal of Hydrology, 583, 124609. doi:10.1016/j.jhydrol.2020.124609.

[15] Azis, R., Maricar, F., Thaha, M. A., & Bakri, B. (2024). The Hybrid System of Fluidization and Sediment Flushing for Maintenance Dredging Technique. Civil Engineering Journal (Iran), 10(7), 2275–2292. doi:10.28991/CEJ-2024-010-07-013.

[16] Luan, G., Wang, T., Hou, J., Li, D., Pan, X., Zhang, R., & Han, Z. (2024). A high-resolution water quality model coupled sediment and suspended sediment module. International Journal of Sediment Research, 39(4), 670–682. doi:10.1016/j.ijsrc.2024.05.004.

[17] Escauriaza, C., Paola, C., & Voller, V. R. (2017). Computational models of flow, sediment transport and morphodynamics in rivers. Gravel- Bed Rivers: Processes and Disasters, 1-31. doi:10.1002/9781118971437.ch1.

[18] Selim, T., Hesham, M., & Elkiki, M. (2022). Effect of sediment transport on flow characteristics in non-prismatic compound channels. Ain Shams Engineering Journal, 13(6), 101771. doi:10.1016/j.asej.2022.101771.

[19] Ji, U., Julien, P. Y., Park, S., & Kim, B. (2008). Numerical modeling for sedimentation characteristics of the lower Nakong River and sediment dredging effects at the Nakdong River estuary barrage. KSCE Journal of Civil and Environmental Engineering Research, 28(4B), 405-411.

[20] Badan Standarisasi Nasional. (2009). National, Statistics Agency, and SNI Instant Soup. Badan Standarisasi Nasional, Jakarta, Indonesia. (In Indonesian).

[21] Supian, S., Hiwari, H., Ibrahim, T. M., & Subiyanto. (2020). Hydrodynamic model simulation of Cikidang river estuary, pangandaran based on two season in Indonesia. International Journal of Advanced Science and Technology, 29(5), 220–229.

[22] Karamma, R., Pallu, M. S., Thaha, M. A., Hatta, M. P., Mustari, A. S., & Syarif Sukri, A. (2020). Analysis of Longshore Sediment Transport at Theestuaries of Jeneberang River and Tallo River Caused by Waves on Coast of Makassar. IOP Conference Series: Materials Science and Engineering, 797(1), 012010. doi:10.1088/1757-899X/797/1/012010.

[23] Meyer-Peter, E. (1948). Formulas for bed-load transport. International Association for Hydro-Environment Engineering and Research (IAHR), Madrid, Spain.

[24] Einstein, H. A. (1950). The bed-load function for sediment transportation in open channel flows (No. 1026). US Department of Agriculture, Washington, United States.

[25] Frijlink, H. C. (1953). Discussion of the Kalinske, Einstein and Meyer-Peter and Muller (Zürich) sediment discharge formulae, taking into account recent transport measurements in Dutch rivers. Journées de l'hydraulique, 2(1), 98-103. (In French).

[26] DHI Water & Environment. (2011). MIKE FLOOD, Modeling of River Flooding—Step by Step Training Guide; DHI Water & Environment, Hørsholm, Denmark.

[27] Naufalina, N. E., Marwoto, J., & Rochaddi, B. (2022). Analysis of Sediment Distribution Based on Grain Size in Baron Coastal Waters, Gunungkidul Regency, Yogyakarta. Indonesian Journal of Oceanography, 4(2), 61–67. doi:10.14710/ijoce.v4i2.13934.

[28] Nur, A., Suriamihardja, D. A., Thaha, M. A., & Hatta, M. P. (2021). Hydrodynamic Analysis at the Confluence of the Mahakam River and the Karang Mumus Tributary. Design Engineering, 5186-5202.

[29] Kranenborg, J. W. M., Campmans, G. H. P., van der Werf, J. J., McCall, R. T., Reniers, A. J. H. M., & Hulscher, S. J. M. H. (2024). Effects of free surface modelling and wave-breaking turbulence on depth-resolved modelling of sediment transport in the swash zone. Coastal Engineering, 191, 104519. doi:10.1016/j.coastaleng.2024.104519.